Improved lumped electrical characteristic modeling and adaptive forgetting factor recursive least squares-linearized particle swarm optimization full-parameter identification strategy for lithium-ion batteries considering the hysteresis component effect.

XIE, Y., WANG, S., ZHANG, G., FAN, Y., FERNANDEZ, C. and GUERRERO, J.M.

2023

Improved lumped electrical characteristic modeling and adaptive forgetting factor recursive least squares-linearized particle swarm optimization full-parameter identification strategy for lithium-ion batteries considering the hysteresis component effect

Yanxin Xie [a], Shunli Wang [a,b,*], Gexiang Zhang [a], Yongcun Fan [a], Carlos Fernandez [c], Josep M. Guerrero [d]

[a] School of Information Engineering, Southwest University of Science and Technology, Mianyang 621010, China
[b] School of Electrical Engineering, Sichuan University, Chengdu 610065, China
[c] School of Pharmacy and Life Sciences, Robert Gordon University, Aberdeen AB10 7GJ, UK
[d] Department of Energy Technology, Aalborg University, Pontoppidanstraede, 111 9220 Aalborg East, Denmark

* Corresponding author at: School of Information Engineering, Southwest University of Science and Technology, Mianyang 621010, China.
E-mail address: 497420789@qq.com (S. Wang).

A B S T R A C T

Electric vehicles, as a new green mode of transportation, have put forward higher demand indicators for accurate modeling and efficient parameter identification strategies for lithium-ion batteries. In this paper, a lumped electrical characteristic model is constructed for lithium-ion batteries considering the hysteresis component effect based on a proposed adaptive forgetting factor recursive least squares-linearized particle swarm optimization (AFFRLS-LPSO) algorithm with strong working condition characterization capability for full parameter identification. First, to characterize the relationship accurately and intuitively between the external characteristics and the internal state quantities of the battery, the charging and discharging measurement information is captured, and the difference in the open circuit voltage (OCV) caused by the hysteresis phenomenon is resolved. Then, the complex working condition experiments is conducted, and through online inspection of experimental data, the fusion strategy concept is introduced to prevent the phenomenon of "filter saturation" and improve the ability of the algorithm to track the variable characteristic parameters of the battery. The full parameter identification results and terminal voltage tracking effects under different identification strategies are compared. Also, the consistency verification results of the adaptive parameter identification strategy under different working conditions are further analyzed. The experimental results show that the voltage tracking error of the model with an added hysteresis component is significantly smaller than the error without hysteresis. Furthermore, at an ambient temperature of 15 °C, the root mean squared error and mean absolute percentage error of the AFFRLS-LPSO algorithm are reduced by 0.0037 V and 0.300 %, respectively, under the dynamic stress test and Beijing bus dynamic stress test working conditions, and the consistency accuracy of the unconstrained parameter estimation is improved by 9.9 %. The fusion strategy provides a theoretical basis for real-time parameter identification models for lithium-ion batteries with high precision and adaptability for electric vehicles.

Keywords:
Ternary lithium-ion battery; Hysteresis component effect; Lumped electrical characteristic model; Adaptive forgetting factor recursive least squares; Linearized particle swarm optimization

1. Introduction

With the continuous development of new energy vehicles, large-scale energy storage, special robots, and aviation equipment, the demand for battery systems with large capacity, strong endurance, low environmental pollution, a long cycle life, wide operating range, and high reliability continues to increase [1–5]. As a third-generation battery product, lithium-ion batteries are currently the most widely used energy storage system due to their advantages of high energy density, low self- discharge rate, strong charge retention capability, no memory effect, long cycle life, etc. [6,7]. With the deepening of supply-side structural reform as the main line, the whole world comprehensively promotes energy transformation and industrial restructuring and attaches great significance to the development of lithium-ion batteries. It is the main technical feature is the development direction of energy industry innovation.

Accurate state estimation of lithium-ion batteries based on high-precision model construction effectively suppresses inter-unit differences and their significant error accumulation, as well as the problem of unreasonable decay of cycle life, can prevent irreversible damage to batteries due to over-charge and over-discharge, and provides a reliable foundation for efficient and safe lithium-ion battery management [8]. Accurate and effective equivalent circuit modeling (ECM) and its exact mathematical expression are important prerequisites for lithium-ion battery state estimation and battery system safety management. In the process of real-time online collaborative estimation of multi-state parameters, it is very important to establish an appropriate index system. The most common method is to build an ECM and determine the impedance parameters [9,10]. Due to the internal coupled processes involving electrochemical reactions, charge transfer and heat transfer, lithium-ion batteries have strongly nonlinear dynamic characteristics [11]. Meanwhile, their working environment, series-parallel structure, and application scenarios have significant complexity, which further increases the difficulty of mathematical modeling.

At present, considering the different mechanisms of modeling, they are mainly divided into thermal model, electrical property model, the electrothermal coupling model, and the aging model. Since the battery generates heat during operation, the thermal model requires the assumption of the cause of battery heating and assumes that it all originates from the battery core, thus the estimation of the temperature of the battery core may lead to its high estimation value. For a specific ECM, the model parameter identification strategy directly determines the reliability and accuracy of the established model. Model parameter identification is mainly divided into two categories: offline and online. The commonly used offline identification algorithms include impedance spectrum analysis (ISA) method, external characteristic fitting (ECF) method, least square (LS) method and genetic algorithm (GA) [12–17]. Wang et al. [18] passed the HPPC test and used the point calculation method to identify the model parameters for data processing. However, this method requires a large amount of experimental data to support is, and there are many external factors affecting battery operating characteristics, which greatly limits the accuracy of modeling. Yang et al. [19] used a simulated annealing-particle swarm optimization (SA-PSO) algorithm for offline parameter identification, but the amount of stored data is large and the operation rate is reduced. Offline identification requires that the identified object be separated from the entire system, and then a large amount of input and output data are stored, and data processing is performed according to a certain identification algorithm. The works of Tian et al. and Wang et al. endow the model with a certain physical meaning to better study the relationship between the battery model and the internal properties. Although this method has high precision, the parameters cannot change in real time with time [20,21]. Offline identification methods are time and resource intensive, can be limited by sample data, are not applicable to dynamic environments, and rely on specialized skills with questionable credibility.

The online identification algorithm can obtain the identification results in real time because it does not need to know the experimental data in advance, so this kind of algorithm is widely used in the process of complex influencing factors and random changes in working conditions [22]. Commonly used online identification algorithms include recursive least squares (RLS), forgetting factor recursive least squares (FFRLS), and other least squares derivatives [23–26]. Wu et al. [27] proposed an online identification algorithm called adaptive forgetting factor recursive augmented least squares (AFFRALS), which can effectively solve the problem of dynamic allocation of data weights under the influence of non-Gaussian white noise. However, it does not consider the influence of the internal characteristics of the battery, making the model local defects. Ouyang et al. [28] proposed a robust recursive least squares al-gorithm to extract model parameters online. Even if there are abnormal values in the battery measurement signal, the parameter identification performance can be effectively guaranteed, but the identification accuracy needs to be improved. The work of Xiong et al. [29] and Wang et al. [30] further optimized the online parameter identification strategy to accurately simulate the internal dynamic characteristics of lithium-ion batteries, but ignored the physical meaning of the battery itself.

Therefore, considering the influence of internal electrochemical mechanisms, materials, spectrum, and internal diffusion effects of lithium-ion batteries, a battery model that meets the requirements of accuracy, complexity, and computation is constructed. Intending to seek the optimal solution of the model structure under various constraints, it monitors and simulates the battery's dynamic characteristics and complex reaction mechanism, and provides accurate and effective input parameters for battery state estimation and life prediction [31–34].

Different types of models have been developed to estimate the states of batteries, but many challenges remain. For instance, (1) Balance between accuracy and computational speed: Battery models need to have high accuracy to ensure that the simulation results match the actual situation. However, more detailed models need to consider more parameters, which will increase the computational complexity, while simplified models will ignore some important influencing factors. Therefore, a balance between accuracy and computational speed is needed when building the model. (2) Real-time: The battery model needs to be able to be used in a real-time environment. This means that the model needs to be responsive with sufficient accuracy for real-time control. (3) Scalability: With the emergence of new battery technologies, the battery model needs to be scalable to accommodate different application scenarios. Therefore, we need to validate and test the model to ensure its accuracy and reliability under different operating conditions. (4) Data acquisition: The battery model needs a large amount of data support, including battery composition, performance parameters, working conditions, etc. The difficulty and cost of this data acquisition are also one of the challenges of battery model construction.

The method proposed in this work for original contributions differs from that used in the preceding literature. First, the differences between battery charge and discharge are introduced into a lumped electrical characteristic model considering the influence of the hysteresis component and constructed based on an adaptive forgetting factor recursive least squares-linearized particle swarm optimization (AFFRLS- LPSO) algorithm. Secondly, to make up for the "data saturation" shortcomings of the traditional model parameter identification algorithm, the fusion strategy concept is introduced for the intelligent algorithm used for optimization in the identification of the full parameters of the battery. Finally, to characterize the parameters with clear physical meaning, normalization is performed to verify the accuracy of the identification results on long-term scales.

The remainder of this paper is organized as follows. Section 2 demonstrates lumped electrical characteristics model and the AFFRLS-LPSO parameter identification strategy. The Section 3 introduces the battery experiment platform, as well as provides experimental results and further discussion. Finally, Section 5 is the conclusion of the paper.

2. Model building and identification strategy

2.1. Lumped electrical characteristic modeling considering hysteresis

A lithium-ion battery is a high-energy secondary battery, which is a general term for batteries with lithium-ion intercalation compounds as positive electrode materials. Its energy conversion mechanism involves the multi-level transport process of carriers in components such as a positive electrode, a negative electrode, separator, and electrolyte, which realizes energy conversion through the transfer of carriers between positive and negative electrodes [35,36]. The negative electrode of a lithium-ion battery is graphite, which is often used as the base material for the oxidation reaction against discharge because of its multi-layer structure and ability to accommodate lithium ions [37]. The positive electrode is a transition metal oxide for the reduction reaction to occur during discharge. The model structure of the electrical properties of the lithium-ion battery particle set is shown in Fig. 1.

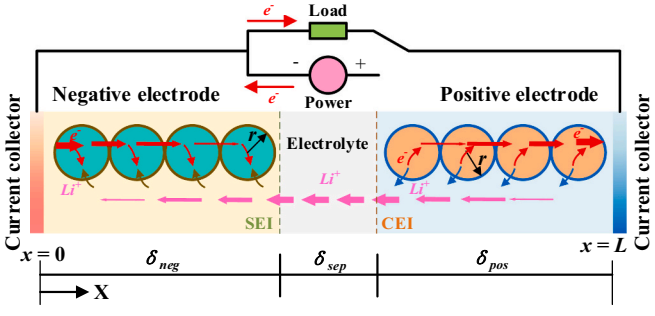

Fig. 1. Lumped electrical characteristic model structure.

As shown in Fig. 1, throughout the charge and discharge process, the carbon material itself provides lattice vacancies, and Li^+ is repeatedly extracted and intercalated between the positive and negative electrodes. The description of these carrier dynamic transfer processes is to build a battery model that is highly correlated with the internal properties. At present, ECMs that describe electrochemical properties through multiple combinations of simple components such as resistors, capacitors, and inductors are widely used. The modeling process is based on experimental data and can be used to characterize electrochemical properties, thermal behavior, temperature, and aging effects as a function of charge-discharge current and closed-circuit voltage. Meanwhile, the true output value of the terminal voltage is estimated under a certain current input. Therefore, a battery model that effectively balances complexity and accuracy is of great significance for the estimation of each state quantity in the battery management system.

At present, the ampere-hour integration method is the methodology commonly used for state of charge (SOC) estimation, and its estimation formula is shown in Eq. (1) [38,39].

$$\frac{\int_{t_0}^{t} \eta \cdot I(\tau) d\tau}{C_e} \tag{1}$$

In Eq. (1), SOC(t_0) denotes the initial value of SOC, C_e denotes the battery rated capacity, η is the Coulomb coefficient, and $I(\tau)$ is the function of charge and discharge current versus time. Based on Eq. (1), the discretized recursive form of SOC is shown in Eq. (2).

$$z_k = z_{k-1} - \eta I_{k-1} \Delta t / C_e \tag{2}$$

In Eq. (2), z_k and z_{k-1} indicate SOC values at k and k-1 respectively, and Δt indicates the sampling time interval.

Due to the complex electrochemical reaction, charge transfer, heat transfer, and other coupled processes involved in the interior of the battery, it has strong nonlinear dynamic characteristics. For the analysis of the internal reaction mechanism of the battery, establishing an ECM can reduce the energy loss during the experiment [40]. Compared with traditional secondary batteries, lithium-ion batteries have the advantages of high energy density, long cycle life, and high computational cost. The method of constructing battery ECMs and using them as core energy storage components has become an effective way to solve the problem of reliable energy supplies [41]. The commonly used battery models can be divided into four categories: thermal model, electrical characteristic model, electrothermal coupled model, and aging model.

In this paper, considering the difference in battery OCV caused by hysteresis, a lumped electrical characteristic model integrating multi- stage parameters is constructed. The model structure is shown in Fig. 2.

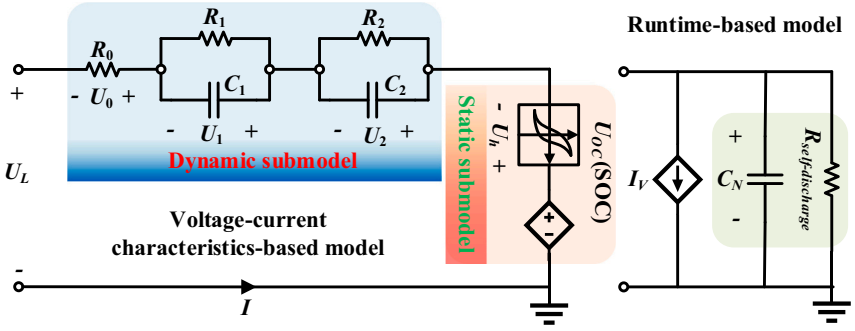

Fig. 2. The schematic diagram of second order RC hysteresis model.

In Fig. 2, U_{OC}(SOC) stands for the static OCV of a lithium-ion battery. R_0 indicates the ohmic internal resistance, the instantaneous change in the terminal voltage caused by the reaction current. R_1 and R_2 express the polarization resistance of the battery. C_1 and C_2 express the polarized capacitance of the battery. R_1, R_2, C_1, and C_2 denote the battery's static characteristics and jointly reflect the polarization effect caused by the current change. Hyst is a hysteresis module, which is used to describe the battery hysteresis effect, and its hysteresis voltage is represented by Uh. I denotes the battery load current, and the positive direction in this paper represents the discharge. UL represents the battery's load terminal voltage.

Based on Fig. 2, it is divided into two modules: runtime-based model and voltage-current characteristics-based model. The first part models the capacity, SOC, and runtime of a lithium-ion battery, which consists of a capacitor, a current-controlled current source, and a self-discharge resistor. The second part can be divided into static sub-model and dynamic sub-model. The static sub-model shows the battery electromotive force, providing the energy loss of the external circuit. When the two parallel circuits of resistance and capacitance in the dynamic sub-model describe the highly nonlinear dynamic characteristics of the battery, the polarization effect of the charging and discharging process of the battery cell can be more accurately characterized. Also, the hysteresis caused by the mechanical stress and the distortion of the active electrode material during the battery working process is considered, to realize the precise mathematical expression of the battery working characteristics and the effective extraction of the characteristic information.

2.2. Model-based modular state discrete representation

It is generally believed that the voltage at both ends of the battery is the OCV after the battery is fully put on hold. At this time, the battery has eliminated the influence of polarization and reached a stable state, which is not affected by the charging or discharging current and is only related to the battery material and the SOC. The SOC can be calculated from the OCV, and this process needs to establish a functional relationship between OCV and SOC. There is a corresponding functional relationship between the open circuit voltage U_{OCV} and SOC of the lithium-ion battery, as shown in Eq. (3).

$$U_{OCV}(t) = f(SOC(t)) \tag{3}$$

To determine the functional relationship between the open circuit voltage U_{OCV} and SOC, according to the proposed model, OCV can be approximated as a nonlinear equation related to SOC, as shown in Eq. (4).

$$U_{OCV}(z) = \alpha_0 + \alpha_1 z + \alpha_2 z^2 + \alpha_3 / z + \alpha_4 ln(z) + \alpha_5 ln(1-z) \tag{4}$$

In Eq. (4), z is the battery SOC value, and α_0 to α_6 are parameters describing the relationship between SOC and OCV. For the same single cell, the OCV-SOC curve is relatively stable.

The voltage hysteresis is caused by the relaxation of the polarization of the battery, and it is manifested that the voltage change shows an asynchronous trend relative to the current change, that is, the surface charge-discharge curves do not overlap. Therefore, this study considers the influence of the battery hysteresis effect to better simulate the hysteresis characteristics of the battery, thereby improving the model accuracy. Professor Plett and others in the United States proposed a formula for calculating the hysteresis voltage, as shown in Eq. (5).

$$\dot{h} = -\left|\frac{\eta_i i\gamma}{C_e}\right| h + \left|\frac{\eta_i i\gamma}{C_e}\right| sgn(i) \tag{5}$$

In Eq. (5), h is the hysteresis level, η_i is the charge-discharge efficiency, and γ is the hysteresis factor. Although the calculation formula of the hysteresis level is obtained, since η_i and C_e are unknown parameters, the formula needs to be rearranged, and the differential equation of the hysteresis level is obtained as shown in Eq. (6).

$$\dot{h} = -|\kappa i|h + |\kappa i| sgn(i) \tag{6}$$

κ is the decay factor. Then, according to Kirchhoff's law, the mathematical relationship representation of the lumped electrical characteristic model is obtained, as shown in Eq. (7).

$$\begin{cases} \dot{U}_1 = -\dfrac{1}{R_1 C_1} U_1 + \dfrac{1}{C_1} i \\ \dot{U}_2 = -\dfrac{1}{R_2 C_2} U_2 + \dfrac{1}{C_2} i \\ U_L = U_{OC} + hM - U_1 - U_2 - iR_0 \\ \dot{h} = -|\kappa i|h + |\kappa i| sgn(i) \end{cases} \tag{7}$$

In this paper, half of the hysteresis voltage is set as M, which is used for the correction of the OCV-SOC relationship. During the experiment, the data collection of the voltage and current of the lithium-ion battery is discrete, which leads to the discrete input of the SOC estimation algorithm. Therefore, the continuous data is segmented into a segmented interval, thereby obtaining the model discrete state-space equation shown in Eq. (8).

$$\begin{bmatrix} z_{k+1} \\ U_{1,k+1} \\ U_{2,k+1} \\ h_{k+1} \end{bmatrix} = \begin{bmatrix} 1 & 0 & 0 & 0 \\ 0 & exp(-\Delta t/\tau_1) & 0 & 0 \\ 0 & 0 & exp(-\Delta t/\tau_2) & 0 \\ 0 & 0 & 0 & exp(-|\kappa i_k|\Delta t) \end{bmatrix} \begin{bmatrix} z_k \\ U_{1,k} \\ U_{2,k} \\ h_k \end{bmatrix} + \begin{bmatrix} -\eta\Delta t/C_e & 0 \\ R_1[1 - exp(-\Delta t/\tau_1)] & 0 \\ R_2[1 - exp(-\Delta t/\tau_2)] & 0 \\ 0 & 1 - exp(-|\kappa i_k|\Delta t) \end{bmatrix} \begin{bmatrix} i_k \\ sgn(i_k) \end{bmatrix} \tag{8}$$

In Eq. (8), Δt represents the sampling time interval, $\tau_1 = R_1C_1$, $\tau_2 = R_2C_2$. The model output voltage can be expressed, as shown in Eq. (9).

$$U_{L,k} = U_{OC,k} + h_k M_k - U_{1,k} - U_{2,k} - i_k R_0 \tag{9}$$

According to the different state parameters of the lithium-ion battery in different modes such as charging, discharging, and standing, to improve the simulation accuracy of the model, the OCV is modified, and the calculation formula of M_k is shown in Eq. (10).

$$M_k = \zeta_{SOC}\left(OCV_{chg,k} - OCV_{dchg,k}\right) \tag{10}$$

Among them, $OCV_{chg,k}$ and $OCV_{dchg,k}$ represent the OCV value of the charging and discharging process respectively. ζ_{SOC} is an adjustment coefficient, and piecewise linearization is adopted for the hysteresis voltage and SOC range, so that the model can fully and accurately reproduce the hysteresis characteristics of lithium-ion batteries. Set $U_E = U_L\text{-}U_{OC}\text{-}hM$, then the circuit transfer function in the complex frequency domain is obtained as shown in Eq. (11).

$$\begin{aligned} G(s) = \frac{U_E(s)}{I(s)} &= -\left(R_0 + \frac{R_1}{1 + sR_1C_1} + \frac{R_2}{1 + sR_2C_2}\right) \\ &= -\left(m_1 s^2 + \frac{m_5}{m_2} s + \frac{m_4}{m_2}\right) \Big/ \left(s^2 + \frac{m_3}{m_2} s + \frac{1}{m_2}\right) \end{aligned} \tag{11}$$

The expressions of $m_1 \sim m_5$ in the Eq. (11) are as Eq. (12).

$$\begin{cases} m_1 = R_0, m_2 = R_1C_1R_2C_2 \\ m_3 = R_1C_1 + R_2C_2, m_4 = R_0 + R_1 + R_2 \\ m_5 = R_0R_1C_1 + R_2R_1C_1 + R_0R_2C_2 + R_1R_2C_2 \end{cases} \tag{12}$$

According to the principle of bilinear transformation, let $s=2(1-z^{-1})/[T(1+z^{-1})]$, the Z domain epression of the transfer function is shown in formula Eq. (13).

$$G(z)=\frac{\theta_3+\theta_4 z^{-1}+\theta_5 z^{-2}}{1-\theta_1 z^{-1}-\theta_2 z^{-2}} \tag{13}$$

The expressions of $\theta_1 \sim \theta_5$ in Eq. (13) are as Eq. (14).

$$\begin{cases} \theta_1=-\left(2T^2-8m_2\right)/\left(T^2+2m_3T+4m_2\right) \\ \theta_2=-\left(T^2-2m_3T+4m_2\right)/\left(T^2+2m_3T+4m_2\right) \\ \theta_3=-\left(m_4T^2+2m_5T+4m_1m_2\right)/\left(T^2+2m_3T+4m_2\right) \\ \theta_4=-\left(2m_4T^2-8m_1m_2\right)/\left(T^2+2m_3T+4m_2\right) \\ \theta_5=-\left(m_4T^2-2m_5T+4m_1m_2\right)/\left(T^2+2m_3T+4m_2\right) \end{cases} \tag{14}$$

Therefore, the difference equation of the electrical characteristic model is shown in Eq. (15).

$$U_E(k)=\theta_1U_E(k-1)+\theta_2U_E(k-2)+\theta_3I(k)+\theta_4I(k-1)+\theta_5I(k-2) \tag{15}$$

2.3. Full-parameter adaptive identification strategy

2.3.1. Multi-identification strategy algorithm fusion architecture

Lithium-ion batteries have strong nonlinear dynamic characteristics in charge and discharge operation due to the coupling process of multiple parameters, such as internal electrochemical reaction, charge transfer, carrier transport, and heat transfer. The conventional offline method for real-time tracking of model parameters and feedback correction is lost. Therefore, this paper adopts the full parameter identification method of online detection data and proposes a fusion strategy. The overall research idea is shown in Fig. 3.

As a typical nonlinear system of a lithium-ion battery, the influence of external conditions will make the changes in various parameters of the model extremely sensitive, and may even lead to the results oscillation or divergence. Because of this, this paper proposes an online parameter identification strategy for lithium-ion batteries with good operating condition characterization capabilities. As shown in Fig. 3, the real voltage and current data measured in the experiment are used as the input of the multi-fusion strategy, and the coupling information about R_0 is used as the input parameter of the linearized particle swarm optimization (LPSO) algorithm, and then fed back to the harmony between the model parameters. The above process completes the parameter identification and update in the response to each link based on the adaptive forgetting factor recursive least squares (AFFRLS) and LPSO lower-level algorithms, and realizes the multi-fusion algorithm parameter identification strategy.

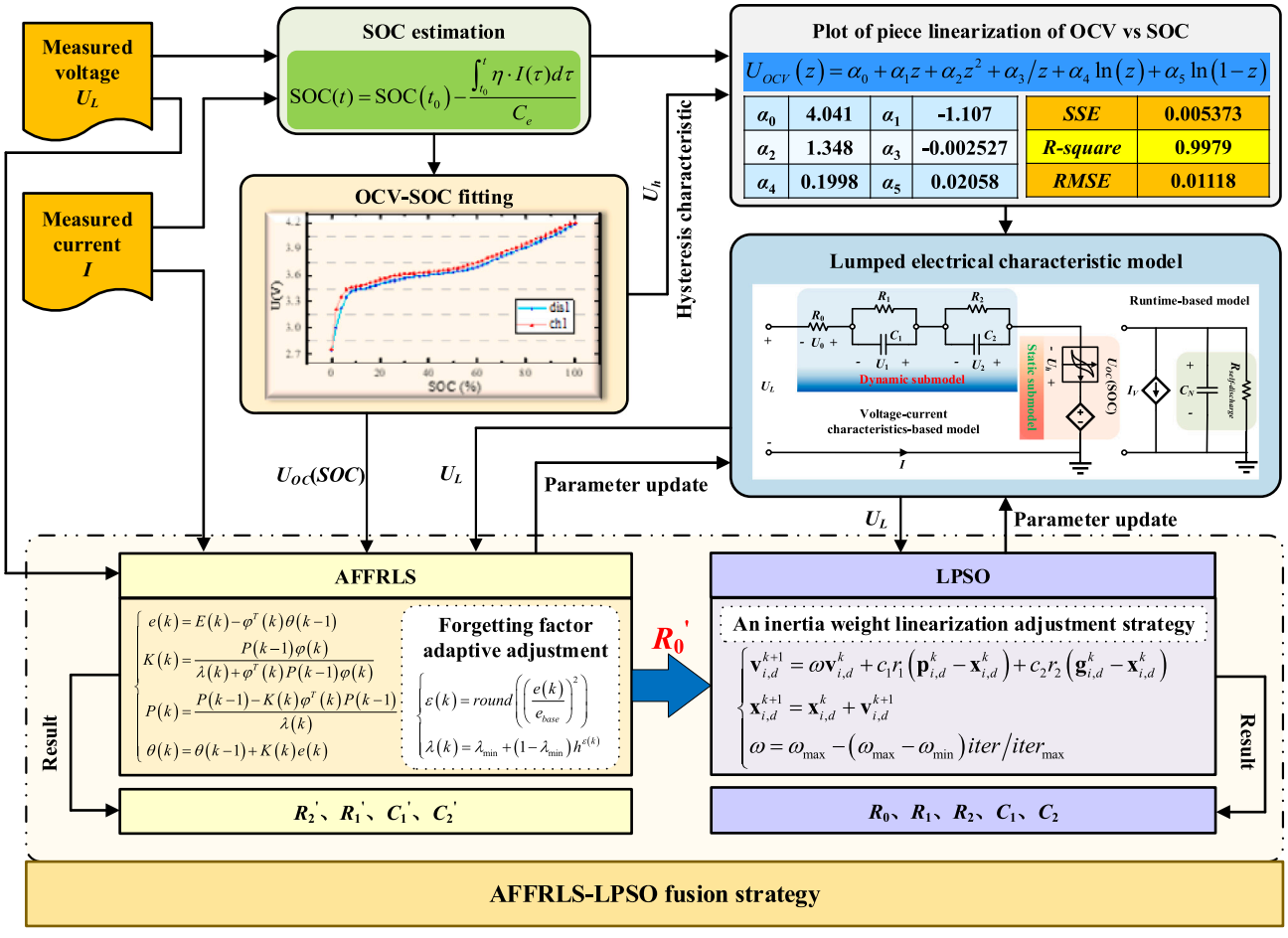

Fig. 3. Full-parameter identification scheme based on AFFRLS-LPSO fusion strategy.

2.3.2. Design of sub-algorithm

2.3.2.1. Adaptive forgetting factor recursive least squares. Aiming at the problem of inaccurate detection of signal feature information by the RLS method, to compensate for the lack of tracking ability of sudden changes and time-varying signals under complex working conditions, an adaptively adjusted weighted forgetting factor λ is introduced based on the optimization of exponential weighting. It solves the requirement that fast-tracking ability and small steady-state error cannot be achieved at the same time under the condition of a fixed forgetting factor, effectively prevents the phenomenon of "filter saturation" in traditional algorithms, and improves the ability of the algorithm to track variable channel parameters. According to the difference equation of the electrical charac-teristic model, the system input matrix is determined, as shown in Eq. (16).

$$\begin{cases} \theta(k) = [\theta_1 \ \ \theta_2 \ \ \theta_3 \ \ \theta_4 \ \ \theta_5]^T \\ \varphi(k) = [\, U_E(k-1) \quad U_E(k-2) \quad I(k) \quad I(k-1) \quad I(k-2) \,]^T \end{cases} \tag{16}$$

In Eq. (16), $\theta(k)$ is the system parameter matrix and $\varphi(k)$ is the system data matrix.

a) Define $e(k)$ as the error between the estimated response of the system and the actual system feedback y(k), which is also the residual, as shown in Eq. (17).

$$e(k) = U_E(k) - \varphi^T(k)\theta(k-1) \tag{17}$$

b) Calculate the parameter matrix θ(k), as shown in Eq. (18).

$$\theta(k) = \theta(k-1) + K(k)e(k) \tag{18}$$

The parameter estimation value at time k is modified based on the estimation at time k-1 by multiplying the innovation and the gain matrix $K(k)$.

c) Update the system gain $K(k)$ as shown in Eq. (19).

$$K(k) = P(k-1)\varphi(k)\left[\lambda(k) + \varphi^T(k)P(k-1)\varphi(k)\right]^{-1} \tag{19}$$

d) Calculate the covariance matrix $P(k)$, as shown in Eq. (20).

$$P(k) = P(k-1) - K(k)\varphi^T(k)P(k-1)/\lambda(k) \tag{20}$$

In this process, the forgetting factor is adaptively adjusted, as shown in Eq. (21).

$$\begin{cases} \varepsilon(k) = round\left(\left(e(k)/e_{base}\right)^2\right) \\ \lambda(k) = \lambda_{\min} + (1-\lambda_{\min})h^{\varepsilon(k)} \end{cases} \tag{21}$$

The *round* function rounds the result to a specified number of digits, and this article sets the rounding to the second digit. The value of the variable forgetting factor can change exponentially linearly with the algorithm's estimation error at the current moment. When the estimation error is larger, the variable forgetting factor is closer to the mini-mum value of the forgetting factor; when the estimation error is smaller, the variable forgetting factor is closer to 1. The AFFRLS identification process is shown in Fig. 4.

The parameters of the lumped electrical characteristic model are separated by parameters, and the function expression between the variables m and θ is obtained from the Eq. (12) and the Eq. (14), as shown in the Eq. (22).

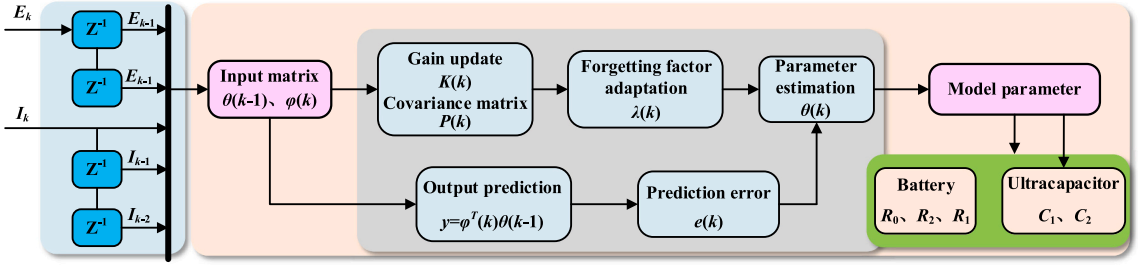

Fig. 4. The flowchart of the adaptive forgetting factor recursive least squares algorithm.

$$\begin{cases} m_1 = (\theta_4 - \theta_3 - \theta_5)/(1 + \theta_1 - \theta_2) \\ m_2 = (1 + \theta_1 - \theta_2)T^2/4(1 - \theta_1 - \theta_2) \\ m_3 = (1 + \theta_1)T/(1 - \theta_1 - \theta_2) \\ m_4 = (-\theta_3 - \theta_4 - \theta_5)/(1 - \theta_1 - \theta_2) \\ m_5 = (\theta_5 - \theta_3)T/(1 - \theta_1 - \theta_2) \end{cases} \tag{22}$$

Assuming $\tau_1 = \left(m_3 + \sqrt{m_3{}^2 - 4b}\right)/2, \tau_2 = \left(m_3 - \sqrt{m_3{}^2 - 4b}\right)/2,$ then the various parameter expressions of the model are obtained as shown in Eq. (23).

$$\begin{cases} R_0 = m_1, R_2 = m_4 - m_1 - R_1 \\ R_1 = [\tau_1(m_4 - m_1) + m_1 m_3 - m_5]/(\tau_1 - \tau_2) \\ C_1 = \tau_1/R_1, C_2 = \tau_2/R_2 \end{cases} \tag{23}$$

The above steps can identify the model full parameters by dynami-cally adjusting the forgetting factor, and simulate the internal electrochemical characteristics of the battery more realistically. It lays a solid foundation for long-term online synchronous estimation of various state parameters of the battery.

2.3.2.2. Linearized particle swarm optimization.

The PSO algorithm is a bionic algorithm that mainly simulates social behaviors such as birds foraging and human cognition. Particles share information only through the current search, and the entire search can converge to the optimal solution faster. To identify the model parameters of the lumped electrical characteristic accurately and quickly, it is often desirable to use a global search first, and then use a local fine search to obtain a high-precision solution, thereby improving the global detection and local mining capabilities of the algorithm. Therefore, based on the traditional PSO algorithm, this paper introduces an inertia weight linearization adjustment strategy to balance the globality of convergence and the speed of convergence, to quickly follow the optimal particle search in the solution space of identification parameters. Assuming that the particle is extended to the *D*-dimensional space search, a population contains *N* particles, and the following four variables are defined.

i. The *i*-th particle position.

$$\mathbf{x}_{i,d} = \begin{bmatrix} x_{i,1} & x_{i,2} & \cdots & x_{i,d} \end{bmatrix} \tag{24}$$

ii. The *i*-th particle velocity.

$$\mathbf{v}_{i,d} = \begin{bmatrix} v_{i,1} & v_{i,2} & \cdots & v_{i,d} \end{bmatrix} \tag{25}$$

iii. The optimal position searched by the *i*-th particle.

$$\mathbf{p}_{i,d} = \begin{bmatrix} p_{i,1} & p_{i,2} & \cdots & p_{i,d} \end{bmatrix} \tag{26}$$

iv. The optimal position searched by the group.

$$\mathbf{g}_{i,d} = \begin{bmatrix} g_{i,1} & g_{i,2} & \cdots & g_{i,d} \end{bmatrix} \tag{27}$$

Therefore, the search speed of the *i*-th particle in the *D*-dimensional space can be represented as shown in Eq. (28).

$$\begin{cases} \mathbf{v}_{i,d}^{k+1} = \mathbf{A}_{i,d}^{k} + \mathbf{B}_{i,d}^{k} + \mathbf{C}_{i,d}^{k} \\ \mathbf{A}_{i,d}^{k} = \omega \mathbf{v}_{i,d}^{k} \\ \mathbf{B}_{i,d}^{k} = c_1 r_1 \left(\mathbf{p}_{i,d}^{k} - \mathbf{x}_{i,d}^{k}\right) \\ \mathbf{C}_{i,d}^{k} = c_2 r_2 \left(\mathbf{g}_{i,d}^{k} - \mathbf{x}_{i,d}^{k}\right) \end{cases} \tag{28}$$

Among them, vk + 1 *i*,*d* shows the *D*-dimensional spatial component of the search velocity vector of particle *i* in the k + 1 iteration process, and xk + 1 *i*,*d* shows the *D*-dimensional spatial component of the particle *i* position vector in the k + 1 iteration process. Ak + 1 *i*,*d* is the inertial part of the current search velocity, which is used to characterize the velocity component of the individual particle affected by the prior conditions. Bk + 1 *i*,*d* is the cognitive part of the particle individual, which is used to optimize the optimal position and direction of the iterative individual. Ck + 1 *i*,*d* is the social cognition part, which transmits the information-sharing mechanism between individuals in the population and is used to adjust the distance and direction between the individual and the optimal position of the group. c_1 and c_2 are the learning factors of individuals and groups, respectively. r_1 and r_2 are random numbers in [0,1], which effectively enhance the randomness of the particle search process. ω is the inertia weight, which can expand the search range of the solution space to a certain extent. The adaptive process of the inertia weight in this paper is shown in Eq. (29).

$$\omega = (\omega_{\max} - \omega_{\min}) exp\left\{ - [iter/(n \cdot iter)]^2 \right\} + \omega_{\min} \tag{29}$$

In Eq. (29), *iter* denotes the current iteration count. This process makes the initial ω of the algorithm larger, the global optimization ability is strong, and it is easy to jump out of the local extremum; while the later ω is smaller, the algorithm is easy to converge. Therefore, the position update of the i-th particle in the D-dimensional space is ob-tained, as shown in Eq. (30).

$$\mathbf{x}_{i,d}^{k+1} = \mathbf{x}_{i,d}^{k} + \mathbf{v}_{i,d}^{k+1} \tag{30}$$

The schematic flowchart of the LPSO algorithm is shown in Fig. 5. To evaluate the excellent performance of the fusion strategy, the root mean squared error (RMSE) and the mean absolute percentage error (MAPE) are used to characterize, and the calculation formula is as follows more intuitively.

$$\begin{cases} RMSE = \sqrt{\dfrac{1}{N}\sum_{i=1}^{N}(y_i - \hat{y}_i)^2} \\ MAPE = \dfrac{100\%}{N}\sum_{i=1}^{N}\left|\dfrac{y_i - \hat{y}_i}{y_i}\right| \end{cases} \tag{31}$$

In the formula, N is the number of samples, y_i is the actual value of the system, and y_i is the estimated value of the system. Eq. (31) can be used to comprehensively evaluate the performance of the algorithm.

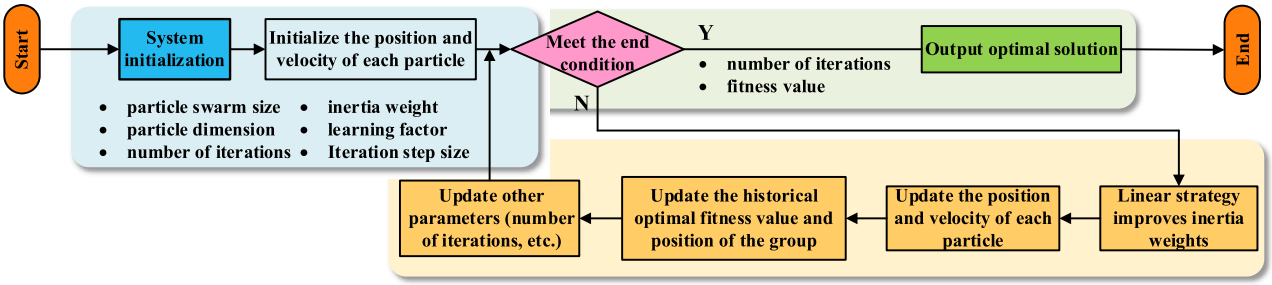

Fig. 5. The flowchart of the linearized particle swarm optimization algorithm.

3. Experiments and results analysis

3.1. Experimental test platform construction

To further verify the accuracy of the battery dynamic characteristics and the lumped electrical characteristic model, this paper selects the 70 Ah ternary lithium-ion battery as the research object and conducts experiments under complex working conditions. The construction of the experimental platform and the detailed parameters of the battery characteristics are shown in Fig. 6.

As shown in Fig. 6, the construction of the experimental platform includes the test battery, the host computer, the power battery charge, and discharge tester (CT-4016-5V100A-NTFA), and the temperature cycle test box (BTKS5-150C). The power battery charge and discharge tester can perform constant current/constant voltage charge and discharge operations on the battery, simulate the real operating conditions of the battery in different scenarios, and output data parameters such as current, voltage, energy, and power of the battery in real-time. The temperature cycle test box can be pulled according to the demand and set a constant temperature value to avoid internal fluctuations caused by environmental factors during the normal operation of the battery. The host computer determines the specific test steps of the battery by setting the corresponding experimental steps under different working conditions, and finally realizes the data transmission between different devices through the TCP/IP, to intuitively read the various types of data collected. Based on the construction of the above experimental platform, various charging and discharging operations of the tested battery can be completed in this paper, providing real test data for the subsequent comprehensive analysis of the algorithm, and using basic experiments and confirmatory experiments to further verify the feasibility of the improved algorithm.

3.2. Comprehensive performance analysis considering hysteresis characteristics

The hysteresis effect is a complex dynamic behavior of the battery, which is manifested as the non-overlapping charge-discharge curves on the surface of the battery. This behavior has the phenomenon of electrode polarization, that is, under the same SOC state, there are different equilibrium potentials, which are all caused by the relaxation of polarization. To verify the model accuracy, the influence of voltage hysteresis is considered in this paper, and the battery is charged and discharged at a rate of 1C under constant temperature conditions to obtain the OCV of the battery in different states. Moreover, the same test was performed at SOC of 40 %, 60 %, and 80 %, that is, when the lithium-ion battery was released or increased its capacity by 20 %, the recorded data was a hysteresis loop, so three hysteresis loops were obtained. Plot the OCV- SOC curve as shown in Fig. 7.

Fig. 7 is the OCV-SOC curve considering the hysteresis characteris-tics, OCV1 represents the open circuit voltage value during the discharge process, OCV2 represents the open circuit voltage value during the charging process, and OCV3 represents the average voltage value during one charge-discharge cycle. D is expressed as the difference between the OCV during charging and discharging. U1 and U2 correspond to the OCV of the charge/discharge process, respectively. The hysteresis loop composed of U3 and U4 is expressed as the terminal voltage variation curve of SOC in the range of 20% to 40%. The hysteresis loop composed of U5 and U6 is expressed as the terminal voltage variation curve of SOC in the range of 40% to 60%. The hystersis loop composed of U7 and U8 is expressed as the terminal voltage variation curve of SOC in the range of 60%~80%. Then, a simplified electrochemical model was fitted to the average OCV and SOC, and the fitting results are shown in Table 1.

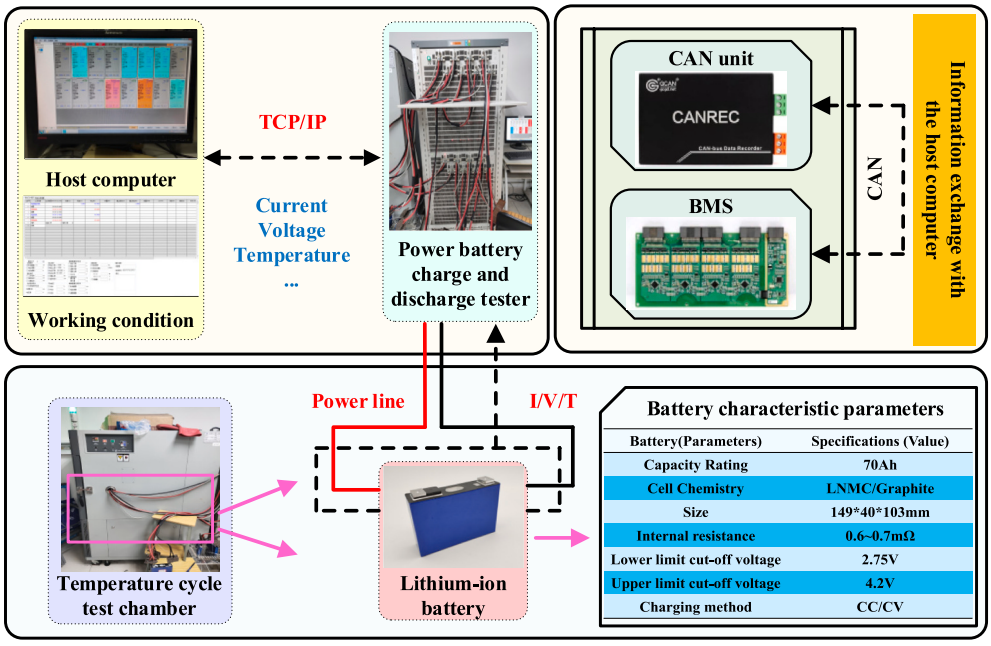

Fig. 6. Construction of experimental platform for battery characteristic test and model test.

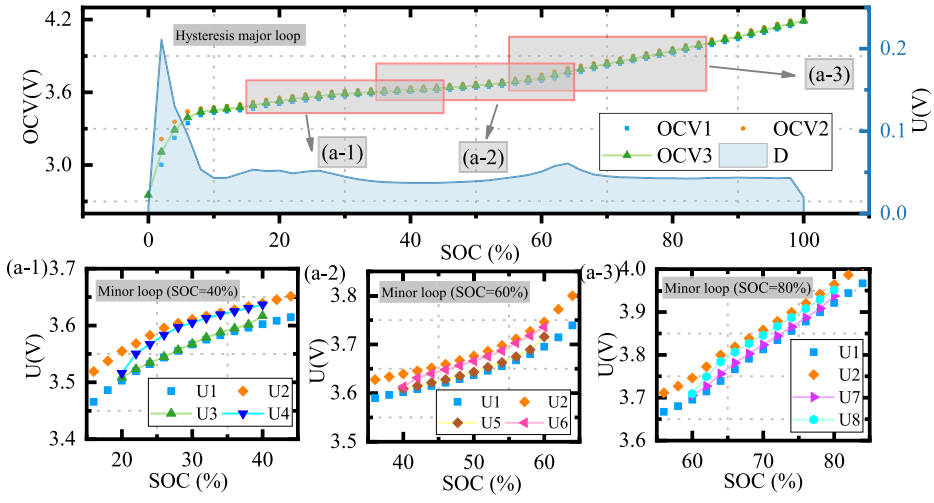

Fig. 7. Plot of piece linearization of OCV vs SOC considering hysteresis characteristics.

In the Table 1, the sum of squares due to error (SSE) describes the sum variance of the fitting method, the coefficient of determination (R- squared) represents the goodness of fit, degree-of-freedom adjusted co-efficient of determination (adjusted R-squared) represents the coeffi-cient of determination of the fitting adjustment, and RMSE represents the root mean square error of the fitting. When the SSE and RMSE values are closer to 0, the fitted data approaches the measured data. When R-squared and adjusted R-squared are closer to 1, the better the fitting equation can interpret the data and the better the fitting effect. This process can well characterize the OCV values corresponding to different SOC values. Given this, removing the influence of the electrode polarization effect, the relationship between the hysteresis voltage U_h and the SOC is obtained as shown in Fig. 8.

Due to the voltage plateau characteristics of lithium-ion batteries, in the voltage plateau region, M is about 50 % of the OCV difference between charge and discharge. In the voltage non-stationary region, the weighting factor is determined by the linear difference. Considering the model accuracy and algorithm complexity, the hysteresis voltage is piecewise linearized according to the SOC range and linearized into a three-segment function, so the OCV-SOC correction strategy is obtained, as shown in Eq. (32).

Table 1
OCV and SOC fitting relationship expression results.

General model	$U_{OCV}(z) = \alpha_0 + \alpha_1 z + \alpha_2 z^2 + \alpha_3/z + \alpha_4 \ln(z) + \alpha_5 \ln(1\text{-}z)$			
Coefficients(with 95% confidence bounds)	$\alpha_0 = 4.041$(3.886, 4.196)	$\alpha_1 = -1.107$ (−1.434, −0.7811)		$\alpha_2 = 1.348$ (1.119, 1.577)
	$\alpha_3 = -0.002527$ (−0.00483, −0.0002235)	$\alpha_4 = 0.1998$ (0.1359, 0.2637)		$\alpha_5 = 0.02058$ (−0.0001217, 0.04128)
Goodness of fit	SSE	R-squared	adjusted R-squared	RMSE
	0.005373	0.9979	0.9977	0.01118

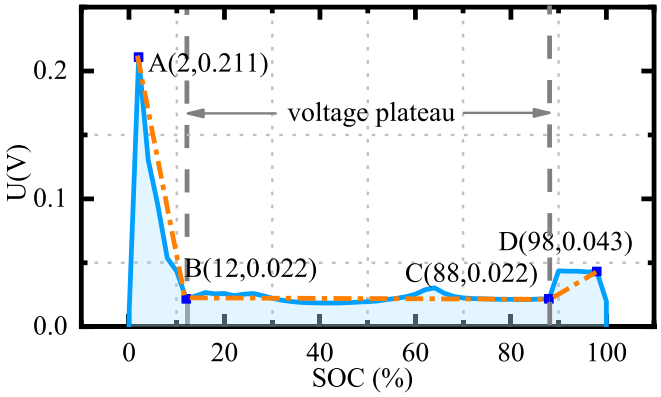

Fig. 8. Plot of hysteresis voltage vs SOC.

$$U_h(k) = \begin{cases} -0.0189z(k) + 0.2498, 2\% \le z(k) \le 12\% \\ M(k), 12\% \le z(k) \le 88\% \\ 0.0021z(k) + 0.1812, 88\% \le z(k) \le 98\% \end{cases} \quad (32)$$

3.3. Statistical analysis of the identified results

According to the constructed lumped electrical characteristic model considering the hysteresis effect, it is necessary to identify the full parameters of the model to reflect the behavioral characteristics of the system, and further illustrate the rationality of the algorithm in char-acterizing the internal effect of the battery. The unknown parameters that need to be identified in this paper include R_0, R_1, R_2, C_1, C_2, and the parameters are identified and the model accuracy is verified under the dynamic stress test (DST) condition. The DST working condition is generally composed of operations such as splitting, cutting, simplifying, and power distribution statistics of the actual working condition. In this paper, the battery is tested for cyclic charging and discharging, and the dynamic change curves of current and voltage at different temperatures are obtained by customizing the DST working conditions in Fig. 9.

For the fusion identification algorithm proposed in this paper, parameter identification is carried out at 15 °C, 25 °C and 35 °C to obtain each state parameter of the model, and the identification results are shown in Fig. 10.

Fig. 10 (a) shows the dynamic adaptive adjustment process of the forgetting factor, and Fig. 10 (b)-(f) shows the identification results of each parameter. In the whole iterative process of the adaptive forgetting factor recursive least squares-linearized particle swarm optimization (AFFRLS-LPSO) algorithm, due to the errors existing in the system itself, there is a large deviation in the early identification stage. However, with the progress of time, each identification result fluctuates within a certain range, indicating that the joint online identification method has high stability. Because of this, using the current data provided by DST con-ditions as input, the experimental parameters based on intermittent charging and discharging correspond to the parameters of the charging and discharging process in Fig. 10. The performance of the ECM is evaluated by comparing the estimated terminal voltage of the simulation model with the measured voltage, and the terminal voltage estimation effect of different identification methods is obtained, as shown in Fig. 11.

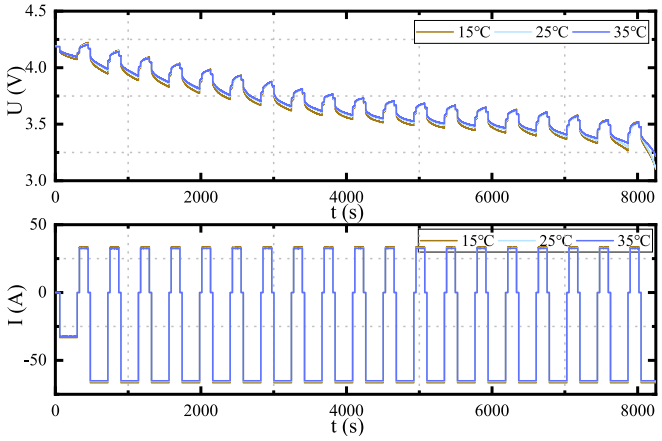

Fig. 9. Experimental test data under DST condition.

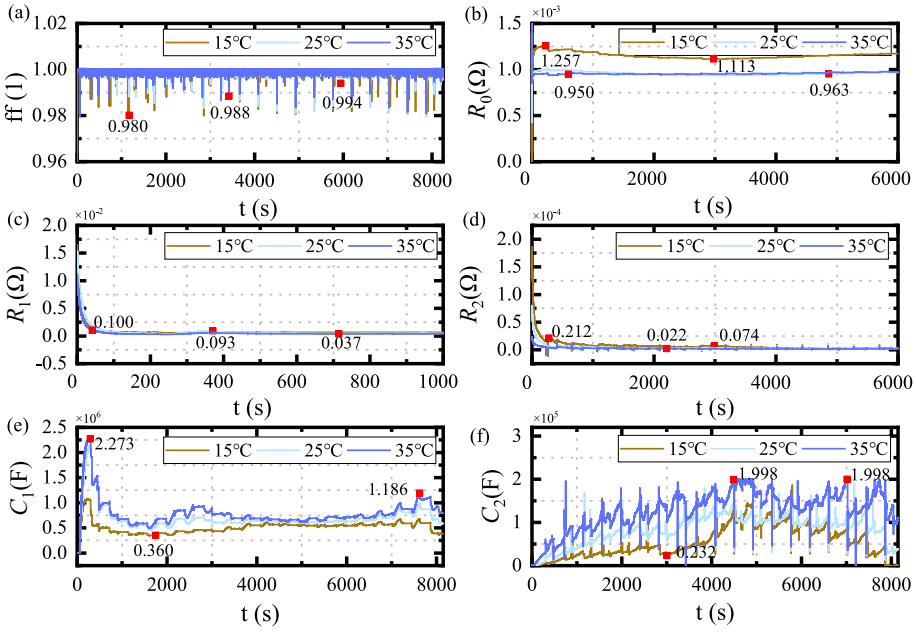

Fig. 10. Full parameter identification results and dynamic forgetting factor adjustment process at different temperatures. (a) Forgetting factor adaptive adjustment curve. (b) R_0 identification result. (c) R_1 identification result. (d) R_2 identification result. (e) C_1 identification result. (f) C_2 identification result.

Fig. 11 (a), (c), and (e) show the results of the simulated versus experimental voltages of the measured lithium-ion battery at different temperatures for the DST conditions. Fig. 11 (b), (d), and (f) show the results of the voltage estimation error of the real-time monitoring parameter model at their corresponding temperatures. According to Fig. 11, the fusion algorithm has a faster convergence rate, and the real voltage value of the lithium-ion battery can be tracked more quickly at the early stage of identification. It can also be seen that the established hysteresis model is closer to the measured value than the simulated voltage waveform without adding hysteresis to the model, and the model without hysteresis cannot simulate the actual battery terminal voltage change in time during the charge/discharge transition. The AFFRLS-LPSO algorithm converges quickly under different working conditions, and the estimates all remain in a stable range with smooth tracking curves. Also, the maximum error of the improved algorithm is more than doubled when comparing with or without adding the hysteresis module and different identification strategies, which verifies its effectiveness and accuracy. With the aging of the lithium-ion battery, except for the end of the discharge stage, the error increases due to the violent electrochemical reaction inside the battery, which is a normal phenomenon. To further verify the universality of the AFFRLS-LPSO algorithm, the experimental steps for the lithium-ion battery test were set with reference to the Beijing bus dynamic stress test (BBDST) condition, and the experimental data under the complex current cycle test was obtained, as shown in Fig. 12.

Similarly, we added different temperatures to the battery model to verify the accuracy of the constructed model by placing the battery in a constant temperature chamber at 15 °C, 25 °C, and 35 °C, respectively, and comparing the model output with the test voltage. Besides, the covariance model without the introduction of hysteresis voltage was also compared to verify the compensation effect of the hysteresis link. Using the experimental data of BBDST dynamic conditions as the excitation, the model verification results and simulation errors are obtained, as shown in Fig. 13.

As can be seen in Fig. 13, the online identification algorithm based on AFFRLS-LPSO still has better estimation accuracy under more complex dynamic conditions, and the relative error of estimated terminal voltage is basically stable within 0.03 V. The model considering the influence of battery hysteresis effect has a significantly smaller voltage tracking error than that without the hysteresis link, and has a significantly smaller relative error compared to the AFFRLS algorithm, with a faster convergence speed and higher stability. Therefore, to further describe the excellent performance of the fusion algorithm in characterizing the full parameters of the model and verifying the accuracy of the model, the Error, RMSE, MAPE, and running time under different dynamic conditions are comprehensively compared. These four indicators are used to quantitatively analyze the accuracy of the model, as shown in Table 2. It should be noted that the total time of this paper is 8250 s under the DST condition and 13,300 s under the BBDST condition. Due to the large increase in the amount of data, the iterative running time of the algorithm is also relatively prolonged.

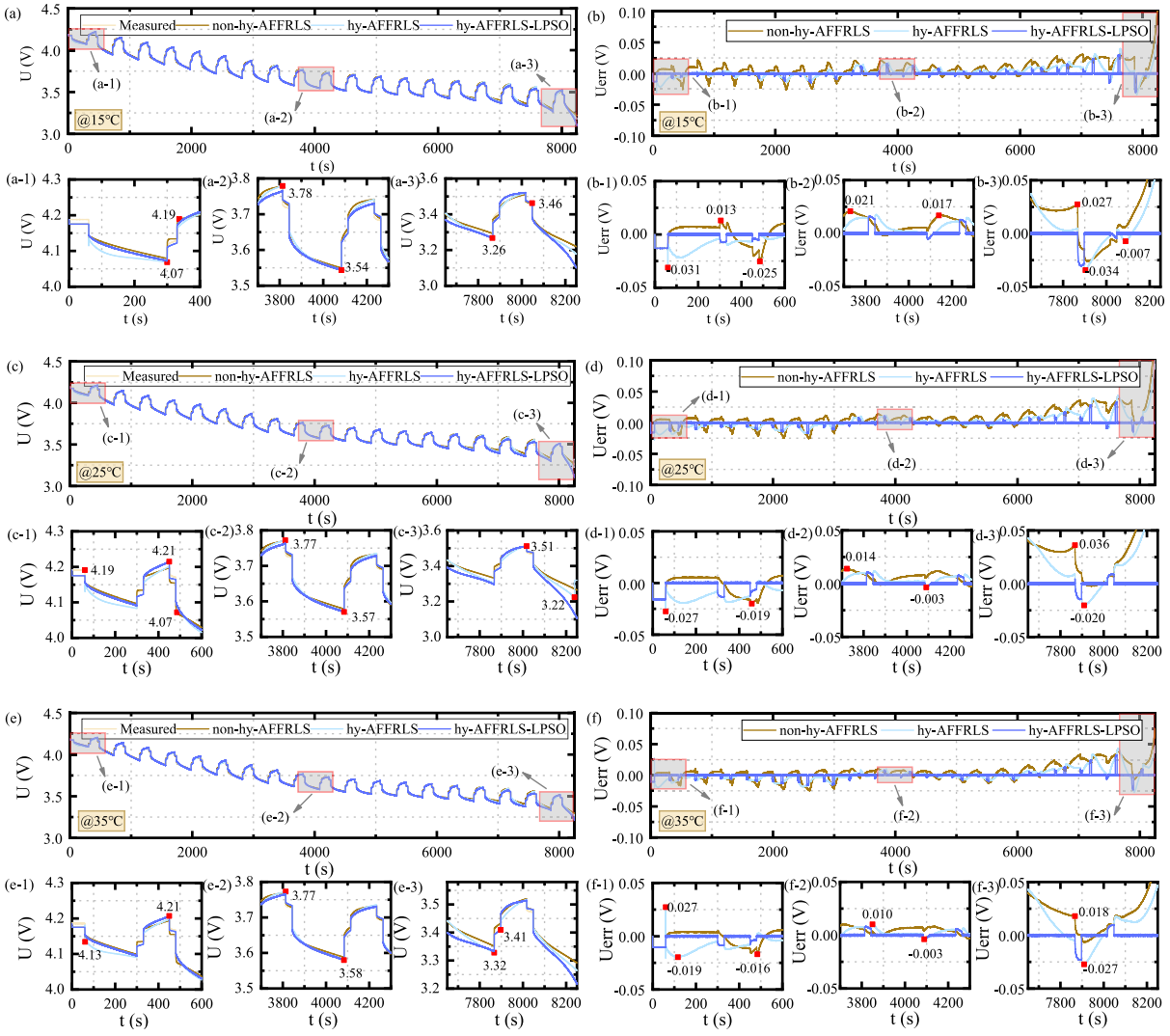

Fig. 11. Comparison of terminal voltage error curves under DST at different temperatures.

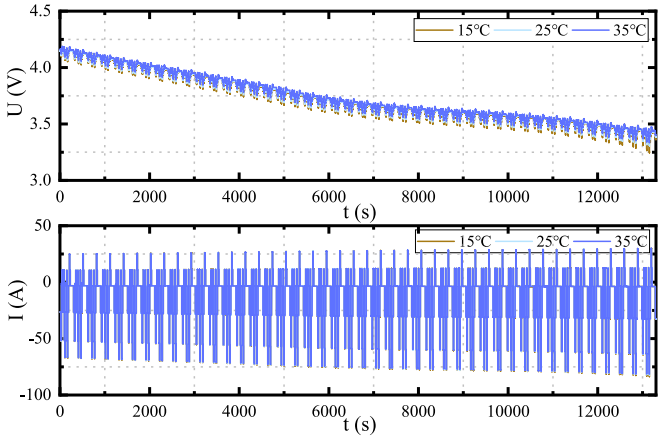

Fig. 12. Experimental test data under BBDST condition.

According to the inter-comparison between the parameters in Table 2, the introduction of hysteresis components more accurately describes the battery behavior, and there is a certain time lag relation-ship between the supplemental potential and the charge state. Taking the ambient temperature of 15 ◦ C as an example, the AFFRLS-LPSO al-gorithm reduces the Error, RMSE and MAPE by 0.0465 V, 0.0192 V and 0.242 %, respectively, and increases the running time

1.881 s compared to the AFFRLS algorithm in the DST condition. In the BBDST condition, the AFFRLS-LPSO algorithm reduces the Error, RMSE and MAPE by 0.0140 V, 0.0037 V and 0.300 %, respectively, and increases the runtime by 1.546 s. Because the fusion algorithm is based on the AFFRLS algorithm, the LPSO algorithm is superimposed, which makes the running time relatively longer, but does not affect the superiority of the comprehensive performance of the proposed algorithm. Hence, the improved algorithm effectively improves the identification accuracy of the ECM parameters, makes the simulated voltage quickly converge to the actual value, and lays a foundation for the accurate evaluation of the state parameters of the subsequent lithium-ion battery.

3.4. Parameter consistency verification analysis

Measuring the correlation between the estimated value of the ter-minal voltage and the actual value is a means of judging the validity of the model and identification strategy. In addition, considering the physical meaning of the internal parameters is also one of the evaluation methods and comprehensively analyzes the consistency of the identification parameters of the multi-fusion strategy under different working conditions. In this paper, the quantitative analysis of all parameters of the model is carried out, and the identification results are normalized to measure the closeness of the correlation of identification parameters under different working conditions at 15 ◦ C. The parameter normalization verification results are shown in Fig. 14.

By standardizing the model parameter data, the verification results under different algorithms shown in Fig. 14 are obtained. Fig. 14 (a) shows the normalization results of the model's full parameters using the single identification strategy algorithm. Fig. 14 (b) shows the normal-ized results of the model's full parameters using the multi-identification strategy algorithm. By comprehensively analyzing the fitness under different conditions, the unconstrained parameter estimation consistency errors of the AFFRLS algorithm are 26.4 % and 12.3 % under the DST and BBDST working conditions, respectively. The unconstrained parameter estimation consistency errors of the AFFRLS-LPSO algorithm are 16.5 % and 9.9 % under the DST and BBDST working conditions, respectively.

Compared with the AFFRLS-LPSO algorithm, the parameter consistency error of the AFFRLS algorithm is larger, which accumulates more errors for the subsequent estimation of the state parameters of the lithium-ion battery. Consequently, the fusion strategy proposed in this paper has far-reaching significance for battery state estimation.

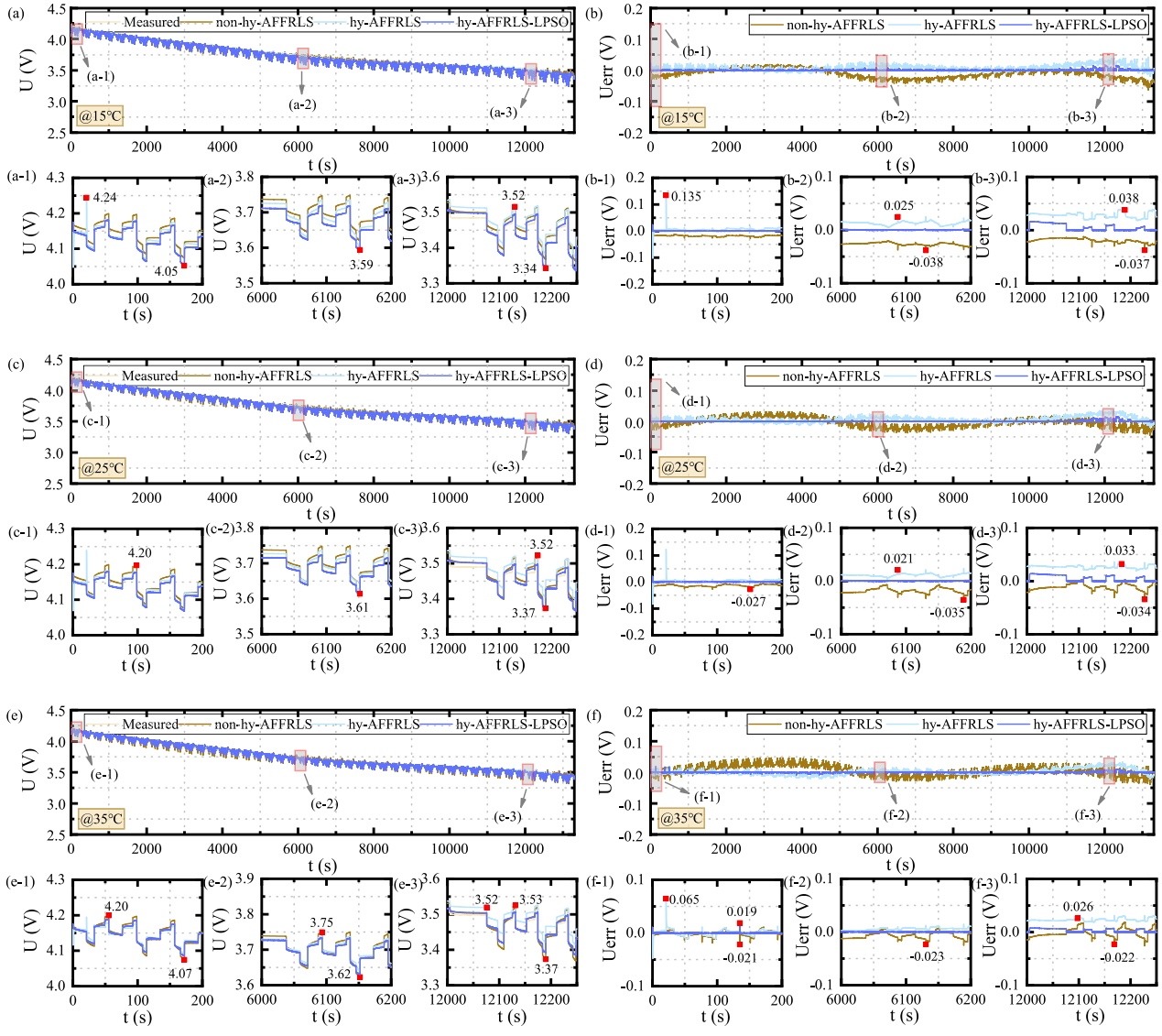

Fig. 13. Comparison of terminal voltage error curves under BBDST at different temperatures.

Table 2
Comparison of Error, RMSE, MAPE, and Running time under DST and BBDST conditions.

Working condition	DST				BBDST			
	15 °C				15 °C			
	Error/V	RMSE/V	MAPE/%	Running time/s	Error/V	RMSE/V	MAPE/%	Running time/s
non-hy-AFFRLS	0.1056	0.0300	0.0042	18.679	0.0424	0.0310	0.0039	26.329
hy-AFFRLS	0.0765	0.0310	0.0031	18.827	0.0257	0.0183	0.0036	28.786
hy-AFFRLS-LPSO	0.0300	0.0118	6.71e-04	20.708	0.0117	0.0146	6.05e-04	30.332

Working condition	DST				BBDST			
	25 °C				25 °C			
	Error/V	RMSE/V	MAPE/%	Running time/s	Error/V	RMSE/V	MAPE/%	Running time/s
non-hy-AFFRLS	0.1080	0.0430	0.0054	19.839	0.0521	0.0440	0.0048	30.112
hy-AFFRLS	0.1071	0.0473	0.0049	19.550	0.0400	0.0334	0.0041	32.871
hy-AFFRLS-LPSO	0.0325	0.0214	0.0012	21.592	0.0143	0.0284	0.0014	35.350

Working condition	DST				BBDST			
	35 °C				35 °C			
	Error/V	RMSE/V	MAPE/%	Running time/s	Error/V	RMSE/V	MAPE/%	Running time/s
non-hy-AFFRLS	0.0723	0.0378	0.0044	22.344	0.0457	0.0304	0.0042	29.034
hy-AFFRLS	0.0469	0.0375	0.0037	19.344	0.0332	0.0296	0.0034	30.861
hy-AFFRLS-LPSO	0.0327	0.0142	8.29e-04	21.285	0.0181	0.0173	8.63e-04	32.880

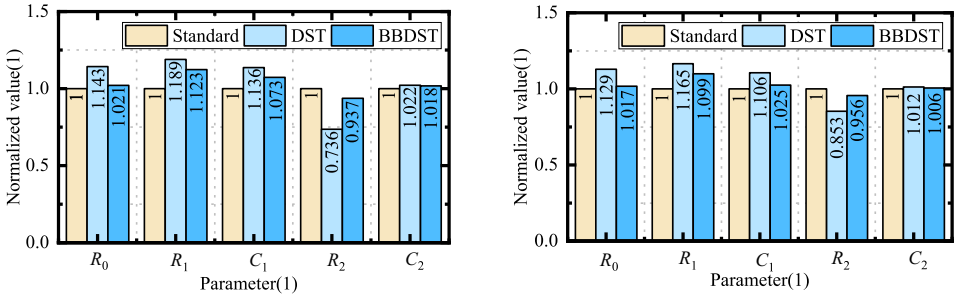

(a) Parameter consistency results under AFFRLS (b) Parameter consistency results under AFFRLS-LPSO

Fig. 14. Normalized check value of each parameter of the model.

4. Conclusion

This paper seeks an accurate modeling method and efficient parameter identification strategy for lithium-ion batteries to clarify the differences between charge and discharge tests. To reduce the model error caused by the difference characteristic, a hysteresis module is introduced to construct a lumped electrical characteristic model considering the influence of the hysteresis component. In addition, a fusion strategy parameter identification based on the AFFRLS optimized by the LPSO algorithm is constructed. This method effectively solves the problem of online synchronous identification of model parameters at long-term scales, balances the globality of convergence and the speed of convergence, quickly tracks the optimal solution in the solution space of identification parameters, and improves the system identification accuracy. Then, the experimental steps of DST and BBDST working conditions are customized, and the correlation between the estimated value of terminal voltage and the actual value of different identification strategies is compared on a long-term scale. The research results fully show that the proposed algorithm has good tracking performance and high generality, and can better characterize the internal dynamic characteristics of the battery, which verifies its superiority over the AFFRLS-LPSO algorithm. Simultaneously, to quantitatively analyze the closeness of the correlation between model parameters under different working conditions, all parameters are normalized. The experimental results show that the unconstrained parameter estimation consistency error is reduced by 9.9 %, and the parameter consistency degree is high. Therefore, this work provides a useful exploration for the reliable modeling and high-precision real-time parameter identification of lithium-ion batteries and lays the foundation for the effective evaluation of subsequent battery states.

CRediT authorship contribution statement

Yanxin Xie: Conceptualization, Methodology, Writing–original draft. **Shunli Wang:** Data curation, Funding acquisition. **Gexiang Zhang:** Validation, Supervision. **Yongcun Fan:** Investigation, Methodology. **Carlos Fernandez:** Formal analysis, Writing–review & editing. **Josep M. Guerrero:** Software, Writing–review & editing.

Declaration of competing interest

The authors declare that they have no known competing financial interests or personal relationships that could have appeared to influence the work reported in this paper.

Data availability

Data will be made available on request.

Acknowledgments

The work is supported by the National Natural Science Foundation of China (No. 62173281, 61801407), Sichuan science and technology program (No. 2019YFG0427), China Scholarship Council (No. 201908515099), and Fund of Robot Technology used for Special Environment Key Laboratory of Sichuan Province (No. 18kftk03). The authors would also like to thank Paul Takyi-Aninakwa at Southwest University of Science and Technology for reviewing & editing.

References

[1] H.Y. Xiong, et al., An energy matching method for battery electric vehicle and hydrogen fuel cell vehicle based on source energy consumption rate, Int. J. Hydrog. Energy 44 (56) (2019) 29733–29742.
[2] J. Galos, et al., Energy storage structural composites with integrated lithium-ion batteries: a review, Adv. Mater. Technol. 6 (8) (2021) 2001059–2001077.
[3] M.K. Hasan, et al., Review of electric vehicle energy storage and management system: standards, issues, and challenges, J. Energy Storage 41 (2021) 102940–102949.
[4] M.R. Li, et al., Multi-step ahead thermal warning network for energy storage system based on the core temperature detection, Sci. Rep. 11 (1) (2021) 15332–15342.
[5] Y. Liu, et al., Advanced lithium primary batteries: key materials, research progresses and challenges, Chem. Rec. (2022) 1–23.
[6] W. Liu, T. Placke, K.T. Chau, Overview of batteries and battery management for electric vehicles, Energy Rep. 8 (2022) 4058–4084.
[7] D. Zhang, et al., Constructing advanced electrode materials for low-temperature lithium-ion batteries: a review, Energy Rep. 8 (2022) 4525–4534.
[8] J.W. Wei, C.L. Chen, G.Z. Dong, Global sensitivity analysis for impedance spectrum identification of lithium-ion batteries using time-domain response, IEEE Trans. Ind. Electron. 70 (4) (2023) 3825–3835.
[9] H.T. Shi, et al., A novel lumped thermal characteristic modeling strategy for the online adaptive temperature and parameter co-estimation of vehicle lithium-ion batteries, J. Energy Storage 50 (2022) 104309–104324.
[10] X.Y. Wang, et al., A review of modeling, acquisition, and application of lithium-ion battery impedance for onboard battery management, Etransportation 7 (2021) 100093–100113.
[11] B.R. Li, et al., A review of solid electrolyte interphase (SEI) and dendrite formation in lithium batteries, Electrochem. Energy Rev. 6 (1) (2023).
[12] L. Chen, et al., Electrochemical model parameter identification of lithium-ion battery with temperature and current dependence, Int. J. Electrochem. Sci. 14 (5) (2019) 4124–4143.
[13] C. Lin, et al., Multi-model probabilities based state fusion estimation method of lithium-ion battery for electric vehicles: state-of-energy, Appl. Energy 194 (2017) 560–568.
[14] Z.B. Wei, et al., Online monitoring of state of charge and capacity loss for vanadium redox flow battery based on autoregressive exogenous modeling, J. Power Sources 402 (2018) 252–262.
[15] L.Y. Ling, Y. Wei, State-of-charge and state-of-health estimation for lithium-ion batteries based on dual fractional-order extended Kalman filter and online parameter identification, IEEE Access 9 (2021) 47588–47602.
[16] X.B. Han, et al., A comparative study of commercial lithium ion battery cycle life in electrical vehicle: aging mechanism identification, J. Power Sources 251 (2014) 38–54.
[17] P. Takyi-Aninakwa, et al., A strong tracking adaptive fading-extended Kalman filter for the state of charge estimation of lithium-ion batteries, Int. J. Energy Res. 46 (12) (2022) 16427–16444.
[18] Q.Q. Wang, et al., An online method to simultaneously identify the parameters and estimate states for lithium ion batteries, Electrochim. Acta 289 (2018) 376–388.
[19] S.C. Yang, et al., A parameter adaptive method for state of charge estimation of lithium-ion batteries with an improved extended Kalman filter, Sci. Rep. 11 (1) (2021) 5805–5819.
[20] N. Tian, et al., One-shot parameter identification of the Thevenin's model for batteries: methods and validation, J. Energy Storage 29 (2020) 101282–101292.
[21] L.M. Wang, et al., State of charge estimation of lithium-ion based on VFFRLS-noise adaptive CKF algorithm, Ind. Eng. Chem. Res. 61 (22) (2022) 7489–7503.
[22] J.P. Tian, et al., Online simultaneous identification of parameters and order of a fractional order battery model, J. Clean. Prod. 247 (2020) 119147–119159.
[23] T.H. Feng, et al., Online identification of lithium-ion battery parameters based on an improved equivalent-circuit model and its implementation on battery state-of- power prediction, J. Power Sources 281 (2015) 192–203.
[24] Q. Zhu, et al., Iterative learning based model identification and state of charge estimation of lithium-ion battery, IET Power Electron. 12 (4) (2019) 852–860.
[25] Z.C. Xu, et al., Co-estimating the state of charge and health of lithium batteries through combining a minimalist electrochemical model and an equivalent circuit model, Energy 240 (2022) 122815–122828.
[26] S.Z. Zhang, N. Peng, X.W. Zhang, An application-oriented multistate estimation framework of lithium-ion battery used in electric vehicles, Int. J. Energy Res. (2021) 1–23.
[27] M.Y. Wu, L.L. Qin, G. Wu, State of charge estimation of power lithium-ion battery based on an affine iterative adaptive extended Kalman filter, J. Energy Storage 51 (2022) 104472–104483.
[28] Q. Ouyang, J. Chen, J. Zheng, State-of-charge observer design for batteries with online model parameter identification: a robust approach, IEEE Trans. Power Electron. 35 (6) (2020) 5820–5831.
[29] R. Xiong, et al., A systematic model-based degradation behavior recognition and health monitoring method for lithium-ion batteries, Appl. Energy 207 (2017) 372–383.
[30] Y.C. Wang, et al., Research on online parameter identification and SOC estimation methods of lithium-ion battery model based on a robustness analysis, Int. J. Energy Res. 45 (15) (2021) 21234–21253.
[31] W. Choi, et al., Modeling and applications of electrochemical impedance spectroscopy (EIS) for lithium-ion batteries, J. Electrochem. Sci. Technol. 11 (1) (2020) 1–13.
[32] Y. Merla, et al., An easy-to-parameterise physics-informed battery model and its application towards lithium-ion battery cell design, diagnosis, and degradation, J. Power Sources 384 (2018) 66–79.
[33] Y. Wu, et al., Research on life cycle SOC estimation method of lithium-ion battery oriented to decoupling temperature, Energy Rep. 8 (2022) 4182–4195.
[34] C.H. Zhang, et al., An adaptive battery capacity estimation method suitable for random charging voltage range in electric vehicles, IEEE Trans. Ind. Electron. 69 (9) (2022) 9121–9132.
[35] C. Norris, et al., Probing the influence of multiscale heterogeneity on effective properties of graphite electrodes, ACS Appl. Mater. Interfaces 14 (1) (2022) 943–953.
[36] L. Hu, et al., Construction of cobalt vacancies in cobalt telluride to induce fast ionic/electronic diffusion kinetics for lithium-ion half/full batteries, J. Mater. Sci. Technol. 127 (2022) 124–132.
[37] J.F. Gao, et al., An interconnected and scalable hollow Si-C nanospheres/graphite composite for high-performance lithium-ion batteries, J. Colloid Interface Sci. 624 (2022) 555–563.
[38] L.C. Ren, et al., An algorithm for state of charge estimation based on a single- particle model, J. Energy Storage 39 (2021) 102644–102652.
[39] L.C. Ren, et al., Comparison of robustness of different state of charge estimation algorithms, J. Power Sources 478 (2020) 228767–228777.
[40] X.T. He, et al., Multi-time scale variable-order equivalent circuit model for virtual battery considering initial polarization condition of lithium-ion battery, Energy 244 (2022) 123084–123098.
[41] L.P. Chen, et al., Adaptive state-of-charge estimation of lithium-ion batteries based on square-root unscented Kalman filter, Energy 252 (2022) 123972–123983.